Available online at website: https://journal.bcrec.id/index.php/bcrec

Bulletin of Chemical Reaction Engineering & Catalysis, 21 (3) 2026, 539-552

Original Research Article

Facile Fabrication of Alginate–BiBDC Composite Beads for Efficient Removal of Methylene Blue from Aqueous Solutions

Nguyen Duy Thanh, Nguyen Truong Thi, Van Cuong Nguyen*, Hoang Ai Le Pham*

Faculty of Chemical Engineering, Industrial University of Ho Chi Minh City, No. 12 Nguyen Van Bao, Hanh Thong Ward, Ho Chi Minh City, Viet Nam.

Received: 9th March 2026; Revised: 25th March 2026; Accepted: 25th March 2026
Available online: 30th March 2026; Published regularly: October 2026

Abstract

Alginate–BiBDC composite beads were produced using Ca^{2+}-mediated ionic crosslinking and assessed for methylene blue (MB) adsorption. FT-IR, XRD, SEM, BET, and TGA validated the effective incorporation of BiBDC and the creation of a porous hybrid network. Among the composites, ALG@BiBDC-2 exhibited the most advantageous textural characteristics (14.16 $m^2.g^{-1}$ surface area, 0.0324 $cm^3.g^{-1}$ pore volume, 16.27 nm pore size), attaining 85.33% methylene blue removal within 60 min. Adsorption was significantly influenced by pH, dose, concentration, and temperature. At a pH_{PZC} of 6.76, electrostatic attraction predominates in the uptake of MB. The adsorption process followed a pseudo-second-order model and a Langmuir isotherm, indicating chemisorption-driven monolayer adsorption. Thermodynamic analysis validated spontaneous and exothermic characteristics. The beads maintained over 60% effectiveness after four cycles, indicating moderate stability and significant promise for treating dye-contaminated wastewater.

Keywords: Alginate; BiBDC; methylene blue; adsorption; wastewater treatment

How to Cite: Thanh, N. D., Thi, N. T., Nguyen, V. C., Pham, H. A. L. (2026). Facile Fabrication of Alginate–BiBDC Composite Beads for Efficient Removal of Methylene Blue from Aqueous Solutions. *Bulletin of Chemical Reaction Engineering & Catalysis*, 21 (3), 539-552. (DOI: 10.9767/bcrec.20680)

Permalink/DOI: https://doi.org/10.9767/bcrec.20680

1. Introduction

Synthetic dyes are widely used in textiles, paper, leather, printing, and other industrial sectors. The discharge of dye-laden effluents into water bodies poses a significant threat to both aquatic ecosystems and human health, as many dyes are persistent, toxic, mutagenic, or carcinogenic [1–4]. Conventional treatment techniques (e.g., coagulation, biological treatments, membrane filtration) often suffer from high cost, incomplete removal, or the generation of secondary waste [5–7]. Hence, developing low-cost, efficient, and reusable adsorbents for dye removal remains a critical research direction [8–10]

Sodium alginate (SA), a natural and biodegradable polysaccharide sourced from brown seaweed, has attracted considerable interest as a sustainable adsorbent matrix for water purification, owing to its plentiful carboxyl (–COO^-), hydroxyl (–OH) functional groups, high biocompatibility, and easy cross-linking ability that promote robust interactions with contaminants, including dyes and heavy metal ions [11]. The adsorption efficiency of sodium alginate can be significantly enhanced when combined with other materials to create composite adsorbents, thereby increasing mechanical stability, porosity, and the availability of functional sites. Recent studies indicate that SA-based composites, including SA/polyvinyl alcohol/κ-carrageenan aerogel beads and SA/MCM-41 hybrid beads, demonstrate significant adsorption capacities for cationic dyes (e.g., methylene blue) and heavy metals (e.g., Cu(II), Pb(II)) via mechanisms such as electrostatic attraction, hydrogen bonding, and

* Corresponding Authors.
Email: nvc@iuh.edu.vn (V.C. Nguyen)
phamhoangaile@iuh.edu.vn (A.L.P. Hoang)

ion exchange, positioning them as viable options for the effective treatment of textile wastewater and mixed pollutant systems [12–14].

Metal–organic frameworks (MOFs) are crystalline, porous materials composed of metal nodes coordinated to organic linkers, offering high surface area, tunable pore structures, and a variety of exposed functional metal sites. These properties render MOFs highly promising for the adsorption and catalysis of pollutants, including dyes [15–17]. Among MOFs, those based on bismuth (Bi-MOFs) have recently emerged owing to their favourable stability, visible-light absorption, and abundant active sites derived from the Bi ions [18–20]. Recent studies have elucidated the synthesis strategies, structural tunability, and structure–property relationships of bismuth-based metal–organic frameworks (Bi-MOFs), demonstrating their high potential for degrading organic pollutants. Due to their low toxicity, diverse coordination environments, and favourable electronic structures, Bi-MOFs have emerged as promising materials for the efficient and sustainable removal of organic contaminants from aqueous systems [18,19,21,22]. For example, the bismuth-terephthalate framework (Bi-BDC) was synthesized via a facile solvothermal route and exhibited ~98 % removal of Rhodamine B (RhB) after 270 min under visible LED irradiation [23,24]. Despite recent progress, the practical application of Bi-MOFs in wastewater treatment is hindered by their limited stability, tendency to agglomerate, and poor reusability in aqueous systems. The integration of Bi-MOFs into biopolymer matrices for textile-dye adsorption remains underexplored. To overcome these limitations, this work develops a stable Bi-MOF-based composite for dye removal, offering a more effective and sustainable approach to treating complex wastewater.

The integration of the structural integrity and substantial adsorption capacity of metal–organic frameworks (MOFs) with the biopolymeric characteristics and processability of alginate enables the production of composite beads that exhibit superior adsorption efficiency, ease of manipulation, and improved recyclability. Alginate beads containing UiO-66 MOF and carboxylated graphene oxide have demonstrated a rapid and effective removal of methylene blue and Cu^{2+} ions in approximately 4 hours via synergistic adsorption mechanisms, including electrostatic interactions, π–π stacking, and pore diffusion [25]. Similarly, MOF/alginate composite beads have exhibited efficient adsorption of Cr(VI), validating the efficacy of this composite method [26]. However, research on alginate-based beads, including bismuth-based metal-organic frameworks such as Bi-BDC, for the adsorption of textile dyes remains scarce. A systematic investigation of ALG@Bi-BDC composites, emphasizing adsorption capacity, kinetics, isotherms, and adsorption mechanisms, is a significant contribution due to the pronounced affinity of Bi-MOFs for organic dyes and the practical benefits of alginate beads, including shape controllability, facile separation, and reusability.

2. Materials and Method

2.1. Materials

Bismuth(III) nitrate pentahydrate ($Bi(NO_3)_3 \cdot 5H_2O$, 98.0%), terephthalic acid (BDC, 98.0%), sodium alginate and rhodamine B (95%) were sourced from Sigma-Aldrich. N,N-dimethylformamide (DMF, 99%) and methanol (MeOH, 99.5%) were purchased from Xilong Scientific Co., Ltd. All chemicals were used as received.

2.2. Methods

2.2.1. Synthesis of BiBDC

Bismuth terephthalate (BiBDC) was synthesised via a solvothermal method. A total of 200 mg of $Bi(NO_3)_3 \cdot 5H_2O$ and 800 mg of terephthalic acid were dissolved in a mixed solvent containing 30 mL of N, N-dimethylformamide and 30 mL of methanol. The mixture was magnetically stirred for 30 min until it was completely dissolved. The resulting clear solution was transferred into a 100 mL Teflon-lined stainless-steel autoclave and subjected to solvothermal treatment at 150 °C for 24 h. After cooling naturally to room temperature, the solid product was collected by filtration and centrifuged at 5500 rpm for 10 min. The obtained solid was washed three times with a DMF/MeOH (1:1, v/v) mixture and once with pure MeOH to remove residual organic species. Finally, the material was vacuum-dried at 80 °C for 24 h, yielding a crystalline BiBDC powder.

2.2.2. Preparation of Alginate@BiBDC composite

A predetermined amount of BiBDC powder was dispersed in 2 mL of deionized (DI) water and ultrasonicated for 30 min to achieve thorough dispersion. In parallel, sodium alginate was dissolved in 20 mL of DI water and then added to the BiBDC suspension under continuous stirring at 300 rpm for 2 h to obtain a homogeneous mixture. The mass ratio of alginate to BiBDC was varied from 10:1 to 10:0 (w/w). The resulting uniform suspension was loaded into a 20 mL syringe and added dropwise into 100 mL of 0.05 M $CaCl_2$ solution using a syringe pump at a controlled flow rate, promoting ionic crosslinking and the formation of hydrogel beads. After 2 h of gelation, the beads were collected by filtration and gently stirred in DI water at 300 rpm for an

additional 2 h to remove residual Ca^{2+} ions. The wet beads were then blotted with filter paper to remove surface water and freeze-dried for 10 h to yield the ALG@BiBDC composite. The resulting composites were designated as ALG@BiBDC-1, ALG@BiBDC-2, and ALG@BiBDC-3, corresponding to ALG-to-BiBDC mass ratios of 10:1, 10:2, and 10:3, respectively.

2.3. Adsorption Studies

2.3.1. Effect of material composition

The adsorption performance of ALG@BiBDC with various composition ratios was evaluated using 0.1 g of adsorbent dispersed in 50 mL of methylene blue (MB) solution (20 $mg.L^{-1}$) in a 100 mL Erlenmeyer flask. The suspensions were shaken at 250 rpm. At predetermined time intervals (0, 15, 30, 45, and 60 min), aliquots were withdrawn, and the residual MB concentration was determined by UV–Vis spectrophotometry at λ = 649 nm.

2.3.2. Effect of adsorbent dosage

To evaluate the influence of adsorbent dosage and identify the optimal amount, different masses of the ALG@BiBDC-2 composite (0.05, 0.075, 0.10, and 0.125 g) were individually added to 50 mL of a methylene blue solution with an initial concentration of 20 $mg.L^{-1}$. The suspensions were agitated at 250 rpm, and aliquots were withdrawn at predetermined time intervals of 15, 30, 45, and 60 min for subsequent spectrophotometric determination of the residual MB concentration.

2.3.3. Effect of initial dye concentration

To investigate the effect of the initial dye concentration on the adsorption performance, the 0.1 g ALG@BiBDC-2 composite was added to 100 mL Erlenmeyer flasks containing 50 mL of methylene blue solutions with initial concentrations of 10, 15, 20, 25, and 30 $mg.L^{-1}$. The resulting suspensions were shaken at 250 rpm, and samples were withdrawn at selected time intervals between 15 and 60 min to monitor the adsorption behaviour.

2.3.4. Effect of solution pH

The influence of solution pH on adsorption performance was examined using 50 mL of a methylene blue solution (20 $mg.L^{-1}$) containing 0.1 g of ALG@BiBDC-2 in 100 mL Erlenmeyer flasks. The initial pH values were adjusted to 3, 5, 7, and 9 by adding dilute HCl or NaOH solutions. The suspensions were agitated at 250 rpm, and aliquots were collected at predetermined time intervals of 7.5, 15, 30, 60, and 60 min for UV–Vis spectrophotometric analysis at 649 nm.

2.3.5. Effect of temperature

The effect of temperature on MB adsorption was investigated by introducing 0.1 g of the ALG@BiBDC composite into 50 mL of MB solution (20 $mg.L^{-1}$, pH 7) at 20, 30, 40, and 50 °C. The mixtures were shaken at 250 rpm, and samples were withdrawn at 15, 30, 45, and 60 min to determine the absorbance and evaluate temperature-dependent adsorption behaviour.

2.3.6. Reusability and structural stability

The reusability of the ALG@BiBDC composite was assessed through repeated adsorption–desorption cycles. After each adsorption run, the spent adsorbent was regenerated by sequential washing with hydrochloric acid solution and ethanol, followed by thorough rinsing with deionized water and drying. The regenerated material was subsequently reused for ten consecutive adsorption cycles under identical experimental conditions.

2.4. Isotherm Models, Kinetic and Thermodynamic Study

Langmuir and Freundlich isotherm models are applied. The Langmuir model assumes monolayer adsorption on a homogeneous surface and is expressed linearly (Equation (1)) as:

$$\frac{C_e}{q_e} = \frac{1}{q_{max} \cdot K_L} + \frac{C_e}{q_{max}} \quad (1)$$

Conversely, the Freundlich model delineates the formation of multilayer adsorption on heterogeneous surfaces, as illustrated by the equation (Equation (2)):

$$\log q_e = log K_F + \frac{1}{n} log C_e \quad (2)$$

where q_{max} (mg/g) is the maximum adsorption capacity, K_L (L/mg) is the Langmuir adsorption constant, K_F (mg/g.(L/mg)$^{1/n}$) is the Freundlich constant related to adsorption capacity, and n (dimensionless) is the Freundlich exponent indicating the favorability of the adsorption process.

The resulting kinetic data were subsequently interpreted using relevant kinetic models:

First-order kinetic model:

$$\ln(q_e - q_t) = \ln q_e - K_1 t \quad (3)$$

Second-order kinetic model:

$$\frac{t}{q_t} = \frac{1}{K_2 q_e^2} + \frac{t}{q_e} \quad (4)$$

Where q_t and q_e are the adsorption capacities at time t and at equilibrium, respectively, and K_1 and K_2 are the rate constants of the pseudo-first-order and pseudo-second-order models. The kinetic parameters are obtained from the linear plots of $\ln(q_e - q_t)$ versus t (first order) and t/q_t versus t (second order). The model that best describes the adsorption process is selected based on the correlation coefficient (R^2).

Furthermore, thermodynamic characteristics such as Gibbs free energy (ΔG°), enthalpy (ΔH°), and entropy (ΔS°) were calculated utilizing the subsequent equations:

$$\Delta G^o = -RT \ln K_c \quad (5)$$

$$\ln K_c = \frac{\Delta S^o}{R} - \frac{\Delta H^o}{RT} \quad (6)$$

In this equation, R represents the ideal gas constant, and T is the temperature (K). A graph of $\ln K_c$ against $1/T$ is used to determine ΔH^o and ΔS^o.

2.5. Material Characterizations

The structural, morphological, and physicochemical characteristics of the synthesized materials were comprehensively investigated using a suite of analytical techniques. Crystalline phases were examined by X-ray diffraction (XRD) employing Cu-Kα radiation over a 2θ range of 5°–80° with a step size of 0.02°. Functional groups and coordination environments were identified using Fourier-transform infrared (FT-IR) spectroscopy on a Bruker Tensor 27 in the range of 4000–500 cm^{-1}. The morphology were characterized by scanning electron microscopy (SEM) using a JEOL JSM-IT800 system.

3. Results and Discussion

3.1. Characterizations of Materials

Figure 1a shows the FT-IR spectra of the alginate bead and ALG@BiBDC composites, confirming the successful formation of alginate–BiBDC hybrid materials. The alginate bead exhibits a broad band at 3200–3500 cm^{-1} corresponding to –OH stretching and characteristic carboxylate bands at ~1600 and ~1420 cm^{-1} attributed to asymmetric and symmetric $-COO^-$ stretching, indicating Ca^{2+}-crosslinked alginate. After incorporation of BiBDC, these bands show slight shifts from 1583 cm^{-1} to 1575 cm^{-1} with increasing BiBDC contents and intensity changes, suggesting coordination interactions between alginate carboxylate groups and Bi^{3+} centers. In addition, the appearance and enhancement of bands in the low-wavenumber region (~520–560 cm^{-1}) are assigned to Bi–O vibrations, confirming the presence of the BiBDC framework. Notably, the band at 1010–1026 cm^{-1} becomes more pronounced in the composites, which is attributed to overlapping C–O–C stretching of the alginate backbone and C–O vibrations of the BDC linker, indicating strong interfacial interactions between the polymer matrix and the MOF phase [27].

The XRD patterns of BiBDC, alginate beads, and ALG@BiBDC composites were obtained within the 2θ range of 10–90° to examine the structural properties of the synthesized materials (Figure 1b). The diffraction pattern of BiBDC exhibits a broad and faint halo primarily centered at 2θ = 20–25°, signifying its essentially amorphous structure with restricted long-range order. The alginate bead displays a distinct broad peak at around 2θ = 21–23°, characteristic of polysaccharide-based materials, attributed to the disordered configuration of polymer chains and intermolecular hydrogen bonding. Following the integration of BiBDC into the alginate matrix, the ALG@BiBDC composites (ALG@BiBDC; ALG@BiBDC-3; ALG@BiBDC-2; ALG@BiBDC-1. respectively) exhibit a broad diffraction band within 2θ = 18–30°, indicating the persistence of the predominant amorphous structure of alginate. Minor discrepancies in peak intensity

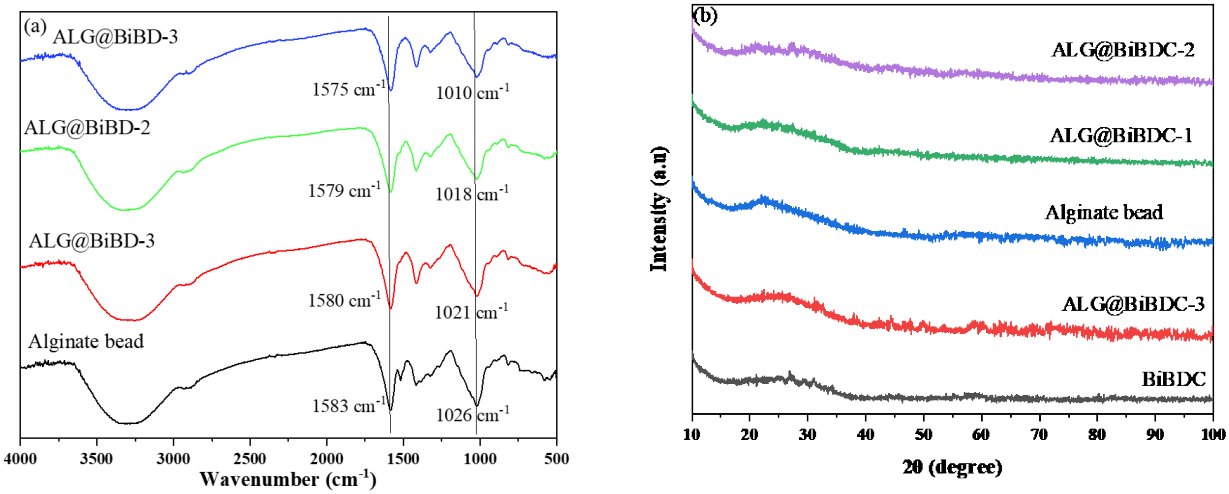

Figure 1. (a) FT-IR spectra and (b) XRD of as-synthesised materials.

are observed among the composites, with ALG@BiBDC-2 exhibiting a comparatively higher intensity near 2θ = 22°, potentially due to enhanced intermolecular interactions or superior dispersion of BiBDC within the alginate matrix. No additional sharp diffraction peaks are observed in the composite samples, indicating that BiBDC is uniformly distributed within the alginate matrix without forming crystalline aggregates.

Thermogravimetric analysis (TGA) reveals distinct decomposition profiles for pristine BiBDC and alginate-modified ALG@BiBDC composites, underscoring the role of alginate in enhancing thermal resilience. All samples exhibit initial mass loss below 200 °C, attributable to the desorption of physisorbed water and residual DMF solvents from the solvothermal synthesis, with losses ranging from 20% to 40%. Thermogravimetric analysis profiles reveal that pristine BiBDC undergoes severe mass loss, approaching ~90% by 600 °C, indicative of the sequential decomposition of BDC linkers and framework collapse into volatile species, leaving minimal Bi_2O_3 residue. In contrast, the ALG@BiBDC composites (10:1, 10:2, 10:3) exhibit significantly moderated degradation, retaining 20-40% char yield at 800 °C owing to alginate's cross-linking reinforcement, which retards organic linker pyrolysis and fosters more robust oxide formation; notably, ALG@BiBDC 10-3 displays the shallowest decline beyond 500 °C, underscoring optimal alginate loading for enhanced decomposition kinetics.

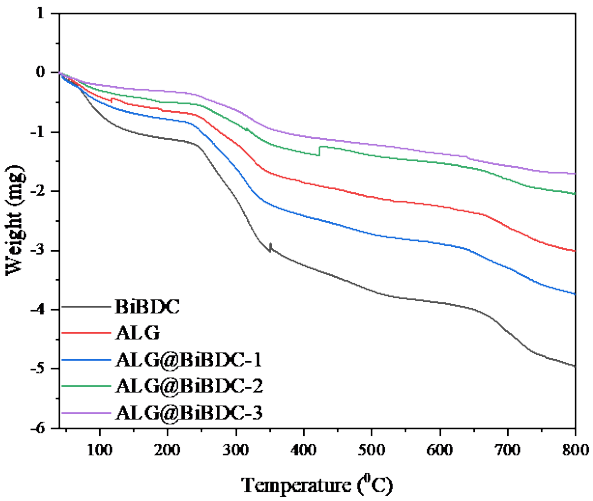

Figure 2. TGA of as-synthesised materials.

Figure 3 illustrates SEM micrographs of the pristine alginate bead and the ALG@BiBDC composites with varying BiBDC loadings, highlighting the morphological changes resulting from the integration of the BiBDC framework. Figure 3a shows that the pure alginate bead has a rather dense, compact surface with low porosity. The surface exhibits a smooth,

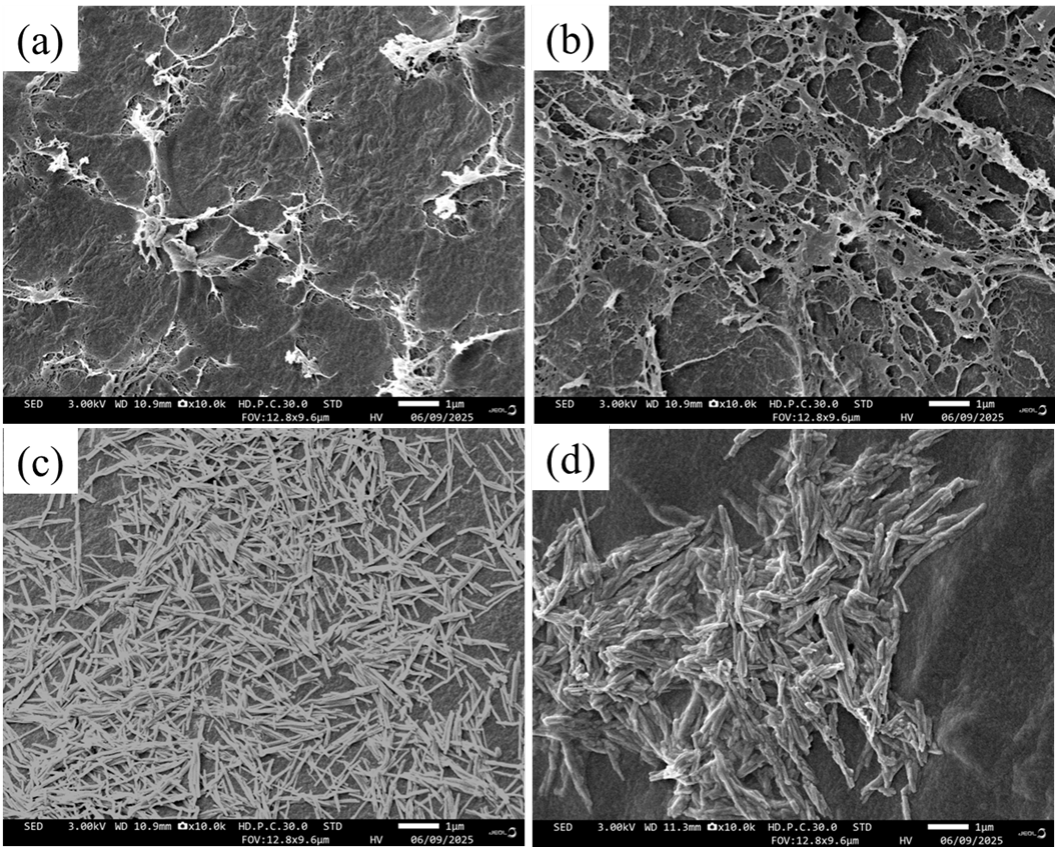

Figure 3. SEM image of (a) alginate bead, (b) ALG@BiBDC-1, (c) ALG@BiBDC-2 and (d) ALG@BiBDC-3.

continuous texture, indicative of ionically crosslinked alginate networks formed during Ca^{2+}-mediated gelation. The introduction of a low amount of BiBDC (ALG@BiBDC-1, Figure 3b) results in a considerable increase in surface roughness and heterogeneity. An interconnected porous network forms, indicating that BiBDC disrupts the dense alginate matrix and facilitates pore development. In ALG@BiBDC-2 (Figure 3c), the composite exhibits a highly developed porous structure with evenly distributed, needle-like BiBDC crystallites integrated within the alginate matrix. The BiBDC buildings are uniformly distributed and interconnected, creating open channels that can significantly enhance mass movement and provide numerous accessible active sites. Conversely, ALG@BiBDC-3 (Figure 3d) demonstrates significant aggregation of BiBDC particles, resulting in densely packed clusters on the alginate surface. The elevated BiBDC concentration leads to partial pore obstruction and diminished structural homogeneity, potentially impeding dye transport and reducing the effective adsorption surface area. This aggregation phenomenon elucidates the reduction in adsorption effectiveness noted at elevated BiBDC loadings [23].

The textural characteristics of the alginate–BiBDC composites, as assessed using N_2 adsorption–desorption studies, exhibit a significant correlation with BiBDC loading and elucidate the observed adsorption behavior (Table 1). The pristine alginate bead exhibits a low BET surface area and a restricted pore volume, indicative of a dense Ca^{2+}-crosslinked polymer network that hinders mass transfer. The addition of BiBDC significantly alters the pore structure, with the ALG@BiBDC-2 composite (ALG : BiBDC = 10:2) exhibiting the greatest BJH pore volume (0.0324 $cm^3.g^{-1}$) and the biggest average pore diameter (16.27 nm), signifying a highly developed mesoporous network. This pore structure facilitates the effective diffusion of methylene blue molecules and increases the accessibility of active adsorption sites, aligning well with its enhanced swelling capacity and adsorption effectiveness. Conversely, inadequate BiBDC loading (10:1) does not yield a continuous porous network, whereas excessive BiBDC incorporation (10:3) leads to particle aggregation and partial pore obstruction, resulting in diminished effective surface area and pore volume. The low specific surface area of the composites is mostly due to the dense polymeric structure of alginate, which, during ionotropic gelation, frequently collapses micro- and mesopores, hence restricting accessible surface area. The integration of BiBDC alters porosity; nonetheless, the alginate matrix partially encapsulates or obstructs MOF particles, hence limiting their inherent surface area. The sodium alginate/graphene oxide composite likewise exhibited a low BET surface area of 2.6 m^2/g [28].

3.2. Swelling Behavior of ALG@BiBDC Composites

The swelling behavior of ALG@BiBDC composite materials with different mixing ratios was systematically investigated, and the results are summarized in Figure 4. Among the evaluated samples, the composite with an ALG-to-BiBDC mass ratio of 10:2 exhibited the highest swelling capacity, attaining a swelling mass of 1.973 g after 60 min and increasing to 2.256 g after 90 min. In contrast, the composite prepared with a higher BiBDC content (10:3) displayed the lowest swelling capacity, with swelling masses of 1.494 g

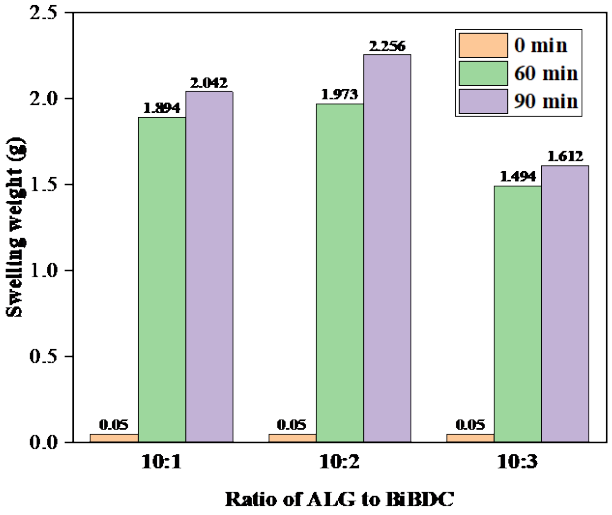

Figure 4. Swelling behavior of ALG@BiBDC composite materials at different ratios (10:1, 10:2, and 10:3) over 0, 60, and 90 min.

Table 1. Textural properties of alginate–BiBDC composites determined by N_2 adsorption–desorption.

Sample	BET surface area ($m^2.g^{-1}$)	BJH pore volume ($cm^3.g^{-1}$)	BJH pore size (nm)
Alginate bead	10.85	0.0166	8.11
ALG@BiBDC-1	2.12	0.0045	12.92
ALG@BiBDC-2	14.16	0.0324	16.27
ALG@BiBDC-3	6.37	0.0093	7.38

and 1.612 g at 60 and 90 min, respectively. The superior swelling performance observed for the 10:2 composite can be attributed to an optimal cross-linking density between the alginate matrix and the BiBDC framework, which facilitates effective water penetration and retention within the polymeric network. Conversely, excessive incorporation of BiBDC at the 10:3 ratio likely introduces rigid inorganic domains that restrict the mobility of alginate chains and reduce the accessibility of hydrophilic functional groups, thereby limiting water uptake. These findings demonstrate that the 10:2 ALG@BiBDC composition provides a favorable balance between structural stability and water absorption capability. Such a balance is particularly beneficial for enhancing mass transfer, adsorption efficiency, and diffusion processes in aqueous environments [29].

3.3. Adsorption Study

3.3.1. Effect of ALG : BiBDC ratio on adsorption efficiency

The effect of alginate and BiBDC mass ratios on the adsorption performance toward methylene blue is shown in Figure 5. For all samples, a rapid increase in adsorption efficiency was observed within the first 30 min, followed by a slower approach to equilibrium after approximately 60 min, indicating fast initial uptake and subsequent saturation of active sites. Among the investigated compositions, the ALG@BiBDC-2 composite (ALG:BiBDC = 10:2) exhibited the highest adsorption efficiency, reaching 85.33% after 60 min, compared with ALG@BiBDC-1 and ALG@BiBDC-3. This enhanced performance is attributed to the synergistic interaction between the alginate matrix and the BiBDC framework, where the polymer provides abundant functional groups (–COOH and –OH) for electrostatic interactions, while the porous BiBDC structure promotes efficient dye diffusion and adsorption. In contrast, composites with lower BiBDC contents (10:0 and 10:1) possessed fewer available active sites, resulting in inferior adsorption efficiency. At higher BiBDC loading (10:3), partial aggregation of the inorganic phase likely occurred, reducing surface accessibility and hindering mass transfer. These results underscore the critical role of achieving an appropriate balance between polymeric support and MOF dispersion to maximize adsorption performance in alginate-based hybrid materials.

The UV–Vis absorption spectra (Figure 6) reveal the time-dependent variation in methylene blue concentration during adsorption onto the ALG@BiBDC-2 composite. The characteristic absorption bands of MB at approximately 664 and 613 nm decreased with increasing contact time, indicating continuous uptake of dye molecules from the aqueous solution. A pronounced decrease in absorbance was observed within the first 15 min, reflecting rapid adsorption driven by the abundance of readily accessible active sites on the composite surface. After 30 min, the rate of absorbance reduction gradually declined, and an almost constant absorbance was attained after 60 min, suggesting that the adsorption process had reached near-equilibrium. This adsorption behavior indicates that rapid initial uptake occurs due to the presence of plentiful vacant sites, followed by a slower stage as these sites become increasingly occupied. The stabilization of the absorbance profile beyond 60 min confirms that equilibrium adsorption is achieved within 60 min, demonstrating the high efficiency and fast adsorption capability of the ALG@BiBDC composite under ambient conditions.

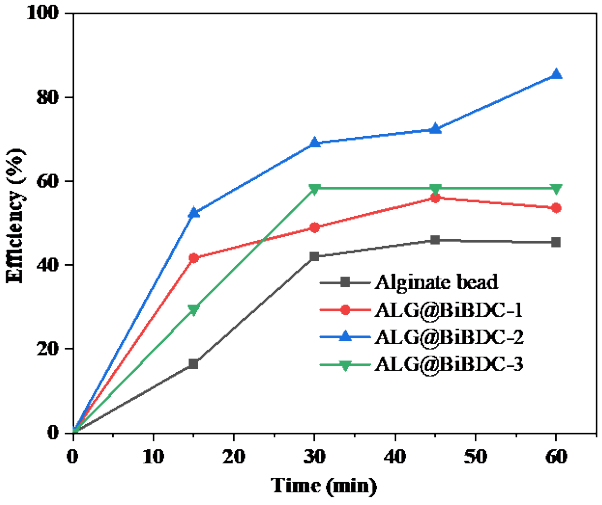

Figure 5. Effect of ALG:BiBDC ratio on the adsorption efficiency of MB versus contact time (conditions: 50 mL MB, 20 mg.L^{-1}, pH ≈ 7, 25 °C).

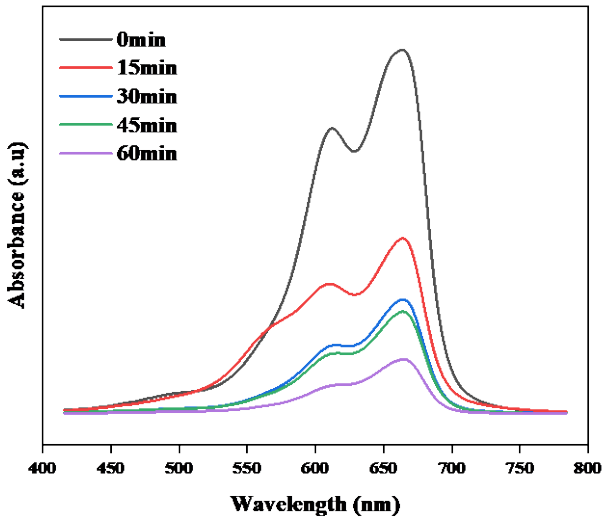

Figure 6. UV–Vis absorption spectra of methylene blue solution at different contact times (0–60 min) over ALG@BiBDC-2 composite.

3.3.2. Effect of adsorbent dosage

The influence of adsorbent dosage on the removal efficiency of methylene blue by the ALG@BiBDC composite was examined over the mass range of 0.05–0.125 g, as presented in Figure 7. The adsorption efficiency increased markedly from 63.05 to 85.33% as the adsorbent mass increased from 0.05 to 0.1 g, which can be attributed to greater availability of active sites and a larger effective surface area at higher dosages, thereby enhancing dye–adsorbent interactions and mass transfer. However, a further increase in the adsorbent mass led to a slight decline in removal efficiency to 81.52%. This reduction is commonly associated with excessive adsorbent loading, which may induce particle aggregation and partial overlap of active sites, consequently decreasing the accessible surface area and impeding dye diffusion. Based on these results, an adsorbent dosage of 0.10 g yielded the highest adsorption efficiency while maintaining cost-effectiveness for subsequent adsorption studies [30].

3.3.3. Effect of initial concentration

The effect of the initial MB concentration on the adsorption performance of the ALG@BiBDC composite was evaluated in the range of 10–30 mg.L^{-1} using 0.10 g of adsorbent with a contact time of 60 min, as shown in Figure 8. The results indicate that the adsorption efficiency increased slightly with increasing MB concentration, reaching a maximum value of 85.33% at 20 mg.L^{-1}. This improvement can be attributed to the enhanced concentration gradient between the bulk solution and the adsorbent surface, which provides a stronger driving force for mass transfer and promotes faster adsorption kinetics. Specifically, when the MB concentration increased from 10 to 20 mg.L^{-1}, the adsorption efficiency rose modestly from 80.39% to 85.33%, suggesting that a sufficient number of active sites were available on the ALG@BiBDC surface to accommodate the additional dye molecules. In contrast, further increases in the initial MB concentration to 25 and 30 mg.L^{-1} resulted in a pronounced decrease in removal efficiency to 68.00% and 60.69%, respectively. This decline is mainly attributed to the saturation of available adsorption sites, leading to excess MB molecules remaining in solution and unable to be effectively adsorbed. Additionally, at higher dye concentrations, possible dye–dye interactions or multilayer adsorption may hinder diffusion into the porous structure of the composite, further

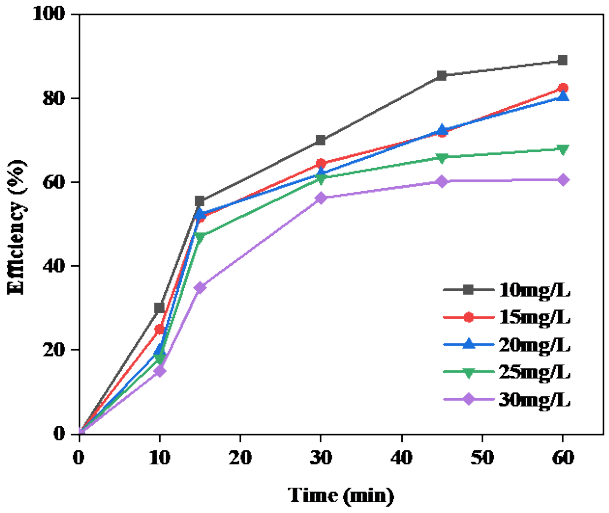

Figure 8. Effect of initial MB concentration on adsorption efficiency of ALG@BiBDC composite as a function of time (10–30 mg.L^{-1}, 0.1 g adsorbent, 50 mL solution) and comparison of equilibrium adsorption efficiencies of MB at different initial concentrations.

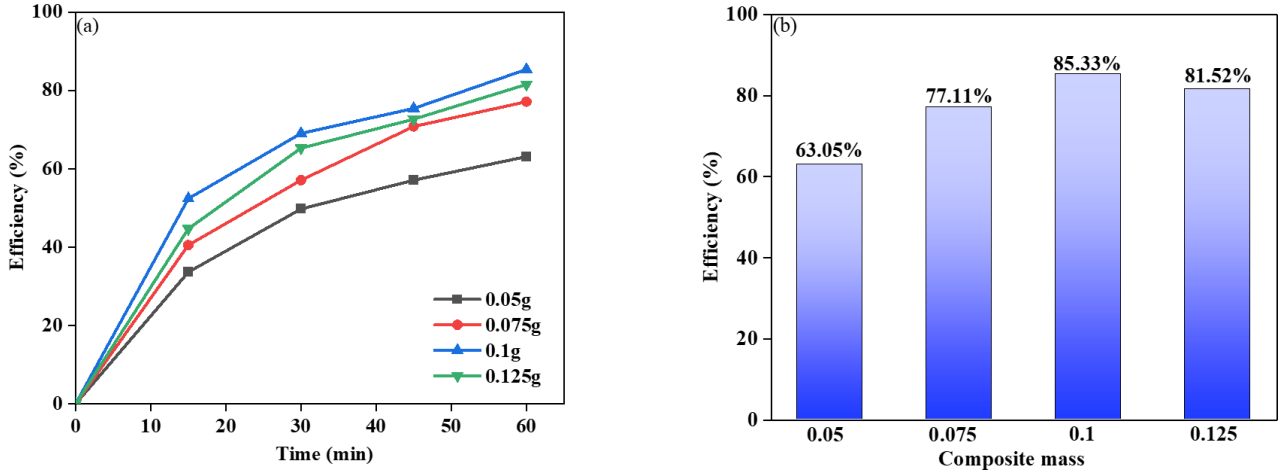

Figure 7. (a) Effect of ALG@BiBDC dosage on adsorption efficiency of MB as a function of contact time (0–60 min, 20 mg.L^{-1}, 50 mL) and (b) comparison of equilibrium adsorption efficiencies of MB at different composite dosages.

limiting adsorption efficiency. Therefore, an initial MB concentration of 20 mg.L^{-1} was identified as optimal for achieving maximum adsorption performance while maintaining effective utilization of the available active sites on the ALG@BiBDC composite [31].

3.3.4. Effect of pH on adsorption efficiency

The influence of solution pH on the adsorption efficiency of methylene blue onto the ALG@BiBDC composite was investigated over a pH range of 3–9, and the corresponding results are depicted in Figure 9. The adsorption performance was highly pH-dependent, with the removal efficiency increasing markedly from 26.45% at pH of 3 to 84.00% at pH of 7. Under strongly acidic conditions, the abundance of H^+ ions leads to the protonation of functional groups on the ALG@BiBDC surface, yielding a positively charged adsorbent. This causes electrostatic repulsion between the adsorbent and the cationic MB molecules, thereby suppressing adsorption and yielding low removal efficiency. As the pH approached neutral conditions, deprotonation of surface functional groups (–COOH and –OH) increased the composite's negative surface charge, facilitating stronger electrostatic attraction to MB^+ ions and thereby improving adsorption efficiency. However, at pH values above 7, a slight decline in removal efficiency was observed (77.98% at pH of 5 and 76.67% at pH of 9), which may be associated with partial dye aggregation and increased competition from OH^- ions for active adsorption sites. Overall, these findings demonstrate that near-neutral conditions (pH ≈ 7) provide the most favorable environment for MB adsorption on ALG@BiBDC, owing to optimal electrostatic interactions between the adsorbent surface and dye molecules [32].

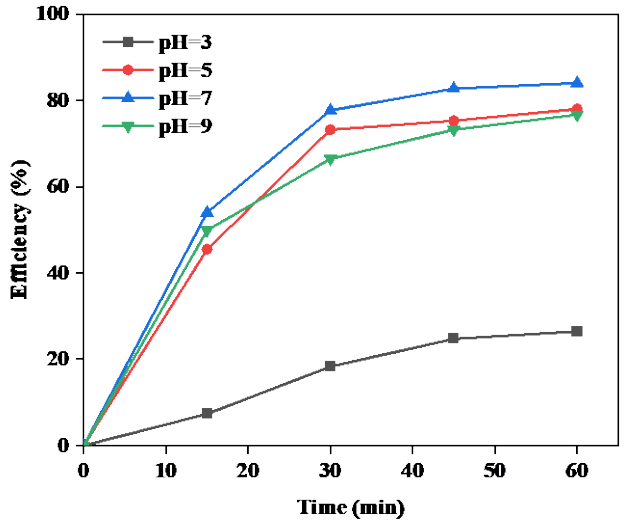

Figure 9. Effect of solution pH on the adsorption efficiency of MB over ALG@BiBDC composite as a function of contact time (0.1 g adsorbent, 20 mg.L^{-1} MB, 50 mL solution).

3.3.5. Effect of temperature on adsorption efficiency

Figure 10 presents the effect of temperature on the adsorption efficiency of the ALG@BiBDC composite with the optimal ALG:BiBDC ratio of 10:2 over the temperature range of 20–50 °C. The highest adsorption efficiencies were achieved at 20 °C and 30 °C, with values of 82.60% and 80.90%, respectively. In contrast, a pronounced decrease in removal efficiency was observed as the temperature increased to 40 °C and 50 °C, with efficiencies declining to 69.45% and 60.33%, respectively. The reduction in adsorption efficiency with increasing temperature suggests that methylene blue adsorption onto ALG@BiBDC is predominantly physisorption-driven. Elevated temperatures increase the thermal motion of MB molecules, thereby weakening van der Waals forces and other weak interactions that support dye retention on the adsorbent surface. Additionally, higher temperatures facilitate desorption and backward diffusion of MB molecules from the composite surface into the bulk solution, further diminishing overall adsorption performance. These observations are in good agreement with previous reports on MB adsorption by alginate-based and biopolymeric adsorbents, which typically exhibit decreased adsorption capacity at higher temperatures, indicating an exothermic adsorption process. Consequently, lower temperatures in the range of 20–30 °C are more favorable for MB adsorption onto ALG@BiBDC, underscoring the suitability of this composite for efficient wastewater treatment under ambient conditions [25].

3.3.6. Reusability of the adsorbent

The reusability of the ALG@BiBDC composite was assessed over five consecutive adsorption–

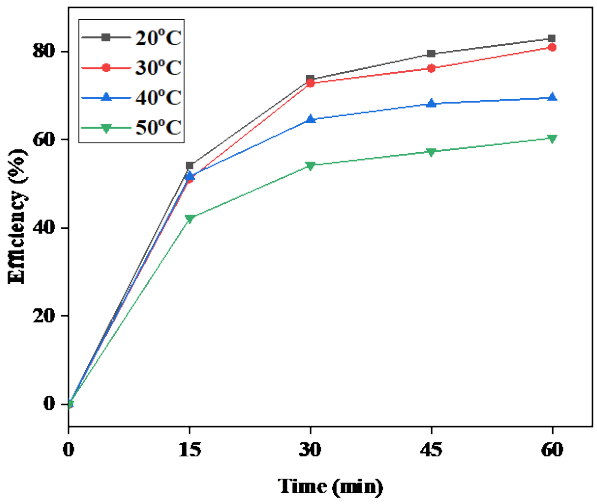

Figure 10. Effect of temperature on methylene blue adsorption efficiency by ALG@BiBDC composite.

desorption cycles, and the corresponding results are presented in Figure 11. A slight decrease in adsorption efficiency was observed during the initial reuse, declining from 85.33% in the first cycle to 83.24% in the second cycle. A more pronounced reduction in performance occurred in subsequent cycles, with efficiencies decreasing to 77.08%, 63.53%, and 32.99% in the third, fourth, and fifth cycles, respectively. The cumulative loss in adsorption efficiency after five cycles indicates that, although ALG@BiBDC exhibits moderate reusability, gradual degradation of active sites and partial loss of structural integrity occur upon repeated use. This decline in performance can be attributed to several factors, including partial blockage of the porous structure or irreversible adsorption of methylene blue molecules, which reduces the number of accessible active sites in later cycles. The reusability results reveal a progressive decrease in adsorption efficiency, suggesting partial degradation of ALG@BiBDC during repeated regeneration. Minor leaching of Bi species is also possible, which would diminish active centers and weaken dye adsorbent interactions. Nevertheless, the composite maintains acceptable performance over five cycles, indicating that the BiBDC framework remains largely intact and that alginate provides mechanical support. Further, the crosslinking or surface stabilization strategies could improve long-term structural stability.

The structural and chemical characteristics of ALG@BiBDC are directly reflected in the adsorption trends. The maximum surface area (14.16 $m^2.g^{-1}$) and largest pore volume of ALG@BiBDC-2 are indicative of its optimal performance, as they facilitate dye diffusion and access to active sites. The increased uptake at low pH is attributed to the strong electrostatic and hydrogen-bond interactions between cationic MB and the –COOH/–OH groups from alginate and BiBDC, as confirmed by FTIR. The rapid initial adsorption rate is supported by SEM images showing an uneven, interconnected surface. The exothermic process is consistent with the decline at elevated temperatures. The observed operational performance is molecularly justified by the porosity, functionality, and morphology of composites.

3.3.7. Determination of the Point of Zero Charge (pH_{PZC})

The point of zero charge (pH_{PZC} of the ALG@BiBDC composite was determined using the pH drift method, as illustrated in Figure 12. The pH_{PZC} value was found to be 6.76, indicating that the surface of ALG@BiBDC is positively charged at solution pH values below 6.76 and negatively charged at pH values above this point. Under acidic conditions ($pH < pH_{PZC}$), the prevalence of protonated surface functional groups ($–OH_2^+$ and $–COOH_2^+$) promotes electrostatic attraction toward anionic species. In contrast, at $pH > pH_{PZC}$ deprotonation of carboxyl and hydroxyl groups generates a negatively charged surface, which favors the adsorption of cationic dyes such as methylene blue. The pH_{PZC} value of 6.76 falls within the near-neutral pH range, suggesting that the ALG@BiBDC composite possesses well-balanced surface charge characteristics. This property enables effective adsorption across a broad pH range, underscoring the suitability of ALG@BiBDC for practical wastewater treatment applications, where pH fluctuations are common.

3.4 Thermodynamic

The thermodynamic parameters provide further insight into the adsorption process. The negative values of ΔG° in the 20–40 °C

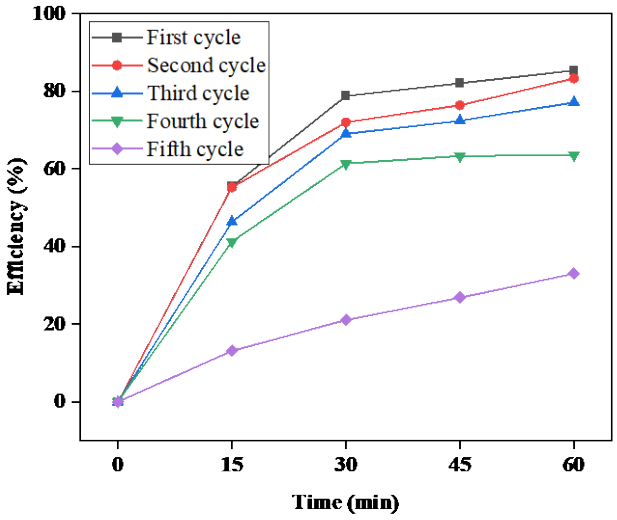

Figure 11. Reusability performance of ALG@BiBDC for methylene blue adsorption over five cycles.

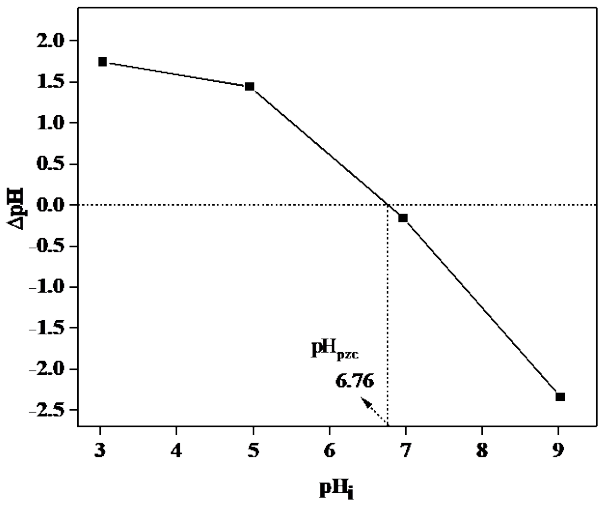

Figure 12. The point of zero charge (pH_{PZC}) of the ALG@BiBDC composite.

temperature range suggest that adsorption is spontaneous, whereas the positive ΔG° at 50 °C suggests a loss of thermodynamic favorability at high temperatures. The thermodynamic analysis confirms that the process is exothermic and spontaneously driven at lower temperatures, with a decreased affinity at higher temperatures.The negative enthalpy change (ΔH° ≈ –34.8 kJ mol^{-1}) indicated that the process is exothermic, which is consistent with a temperature-dependent reduction in adsorption capacity. A ΔH° value shows the mixed process that includes strong physisorption or mild chemisorption. The positive change in entropy (ΔS° = +119.7 $J.mol^{-1}.K^{-1}$) means that the solid–solution interface is more random. This is probably because to desolvation processes and the way water molecules rearrange themselves at the contact during adsorption (Table 2).

3.5. Isothermal and Kinetic Study of Adsorption

Equilibrium adsorption data were further analyzed using Langmuir and Freundlich isotherms. The Langmuir model provided an excellent fit ($R^2 \approx 0.98$), with a monolayer capacity q_{max} of approximately 9.9 $mg.g^{-1}$ and a relatively high K_L demonstrating a strong affinity between the RhB molecules and the composites. Meanwhile, the Freundlich model showed slightly lower correlation ($R^2 \approx 0.95$), although the Freundlich exponent $n = 3.6$ confirms favorable adsorption on mildly heterogeneous sites. The superior performance of the Langmuir model suggests that adsorption occurs predominantly through monolayer coverage on a largely homogeneous surface (Table 3) [33].

The adsorption behaviour was examined by kinetic modelling to elucidate the rate-controlling mechanism. Among the two kinetic models assessed, the pseudo-second-order equation showed the strongest association with the experimental data (R^2 = 0.995–0.998), and the derived q_e values closely matched the experimental data across all initial concentrations. The data suggest that chemisorption, characterized by valence interactions or electron exchange, is the primary rate-limiting factor. The pseudo-first-order model exhibited diminished linearity (R^2 = 0.92–0.96), indicating that physical adsorption alone is insufficient to accurately characterize the system. The rapid absorption observed in the initial 20 min, followed by gradual attainment of equilibrium, indicates a multi-phase mechanism, in which exterior-surface adsorption precedes slower intraparticle diffusion (Table 4).

The adsorption capacity of the Alginate/BiBDC composite beads (9.9 $mg.g^{-1}$ at 20 $mg.L^{-1}$) is moderate compared to other alginate-based systems reported in the literature (Table 5). Pure calcium alginate beads demonstrate minimal adsorption (2.82 $mg.g^{-1}$) owing to their compact structure and low attraction for contaminants [34]. The inclusion of high-surface-area fillers, such as lignin (254.3 $mg.g^{-1}$) [35], graphene oxide (21.33 $mg.g^{-1}$) [36], or MXene (92.17 $mg.g^{-1}$) [37] generally augments adsorption by providing additional functional groups and enhanced porosity. Conversely, the BiBDC loading in this study enhances efficiency (85.33%) but only slightly increases capacity, presumably because the alginate network partially obstructs

Table 2. The thermodynamic variables at different temperatures.

Temperature (K)	ΔG^0 (kJ/mol)	ΔS^0 (kJ/mol·K)	ΔH^0 (kJ/mol)
293	-2.54	119.7	-34.8
303	-1.75		
313	-0.40		
323	0.77		

Table 3. Isotherm parameters for the adsorption.

Langmuir			Freundlich		
$q_{m\ (mg/g)}$	K_L	R^2	K_F	n	R^2
9.9	1.01	0.99	4.5	3.62	0.94

Table 4. Kinetic model parameters of pseudo-first-order and pseudo-second-order.

		Pseudo-first-order			Pseudo-second-order		
C_0 (mg/L)	$q_{e,exp}$ (mg/g)	$q_{e,cal}$ (mg/g)	k_1 (min^{-1})	R^2	$q_{e,cal}$ (mg/g)	k_2 (min^{-1}))	R^2
10	4.5	3.92	0.052	0.961	4.62	0.0068	0.995
15	6.15	5.4	0.048	0.955	6.3	0.0049	0.997
20	8	7.05	0.045	0.948	8.25	0.0036	0.998
25	8.5	7.2	0.041	0.936	8.9	0.0029	0.996
30	9	7.5	0.038	0.921	9.5	0.0024	0.995

pore accessibility and prevents complete exposure of BiBDC active sites. Nonetheless, the composite exhibits a harmonious performance, integrating stability, efficiency, and material simplicity.

4. Conclusion

ALG@BiBDC composite beads were successfully synthesized via a Ca^{2+}-mediated ionic crosslinking approach and evaluated for methylene blue (MB) adsorption. Characterization results (FT-IR, XRD, SEM, BET, and TGA) confirmed the successful incorporation of BiBDC into the alginate matrix and the formation of a mesoporous hybrid structure. Among the prepared materials, the ALG@BiBDC-2 composite (ALG:BiBDC = 10:2) exhibited the most favorable structural properties, including a BET surface area of 14.16 $m^2.g^{-1}$, BJH pore volume of 0.0324 $cm^3.g^{-1}$, and an average pore diameter of 16.27 nm, together with the highest swelling capacity (2.256 g after 90 min). Under optimal conditions (0.1 g adsorbent, 20 $mg.L^{-1}$ MB, pH ≈ 7, 25 °C), the composite achieved 85.33% removal within 60 min. The adsorption process was strongly influenced by pH, dye concentration, dosage, and temperature, with the pH_{PZC} of 6.76 indicating that electrostatic interactions play a key role. The adsorption followed a pseudo-second-order kinetic model, indicating chemisorption-driven interactions, while equilibrium data were best described by the Langmuir isotherm, reflecting monolayer adsorption on energetically uniform sites. Thermodynamic parameters indicated a spontaneous, exothermic process at lower temperatures. The material retained over 60% efficiency after four reuse cycles, demonstrating moderate stability and potential applicability for treating dye-contaminated wastewater.

Acknowledgment

The authors thank the Industrial University of Ho Chi Minh City for their facilities and support.

CRedit Author Statement

Author Contributions: Thanh, N. D.: Methodology, Validation; Thi, N. T. : Methodology, formal analysis; Nguyen, V. C.: Writing review and editing, Data curation; Pham, H. A. L.: Investigation, Writing original draft, formal analysis. All authors have read and agreed to the published version of the manuscript.

References

[1] Kayani, K.F. (2024). Bimetallic metal–organic frameworks (BMOFs) for dye removal: a review. *RSC Advances*, 14(43), 31777–31796. DOI: 10.1039/D4RA06626J.

[2] Liu, Y., Chen, J., Duan, D., Zhang, Z., Liu, C., Cai, W., Zhao, Z. (2024). Environmental Impacts and Biological Technologies Toward Sustainable Treatment of Textile Dyeing Wastewater: A Review. *Sustainability*, 16(24), 10867. DOI: 10.3390/su162410867.

[3] Islam, Md.M., Aidid, A.R., Mohshin, J.N., Mondal, H., Ganguli, S., Chakraborty, A.K. (2025). A critical review on textile dye-containing wastewater: Ecotoxicity, health risks, and remediation strategies for environmental safety. *Cleaner Chemical Engineering*, 11, 100165. DOI: 10.1016/J.CLCE.2025.100165.

[4] Abdullah, H.B., Jusoh, R.B., Safie, W. Bin, Nasaruddin, R.R.B., Khan, M.R., Arifin, M.N. (2026). Modification Strategies of Copper Molybdate-based Photocatalysts for Degradation of Organic Compounds in Wastewater: A Mini Review. *Bulletin of Chemical Reaction Engineering & Catalysis*, 21(2), 244–261. DOI: 10.9767/bcrec.20627.

Table 5. Summary of the adsorption performance of alginate-composite adsorbents for MB.

Materials	Concentration	Adsorption capacity	Adsorption efficiency	References
Calcium alginate beads	30 mg/L	2.82 mg/g	75%	[34]
Sodium alginate/lignin microbeads	100 mg/L	254.3 mg/g	84.8%	[35]
Sodium alginate/graphene oxide hydrogel beads	20 mg/L	21.325 mg/g	98.87	[36]
Ti3C2Tx/sodium alginate gel beads	100 mg/L	92.17 mg/g	81.36%	[37]
Alginate/BiBDC composite beads	20 mg/L	9.9 mg/g	85.33%	This study

[5] Al-Tohamy, R., Ali, S.S., Li, F., Okasha, K.M., Mahmoud, Y.A.-G., Elsamahy, T., Jiao, H., Fu, Y., Sun, J. (2022). A critical review on the treatment of dye-containing wastewater: Ecotoxicological and health concerns of textile dyes and possible remediation approaches for environmental safety. *Ecotoxicology and Environmental Safety*, 231, 113160. DOI: 10.1016/j.ecoenv.2021.113160.

[6] Shabir, M., Yasin, M., Hussain, M., Shafiq, I., Akhter, P., Nizami, A.-S., Jeon, B.-H., Park, Y.-K. (2022). A review on recent advances in the treatment of dye-polluted wastewater. *Journal of Industrial and Engineering Chemistry*, 112, 1–19. DOI: 10.1016/j.jiec.2022.05.013.

[7] Aragaw, T.A. (2024). A review of dye biodegradation in textile wastewater, challenges due to wastewater characteristics, and the potential of alkaliphiles. *Journal of Hazardous Materials Advances*, 16, 100493. DOI: 10.1016/j.hazadv.2024.100493.

[8] Nguyen, T.H.M., Nguyen, V.C., Nguyen, T.H.A. (2025). Photo-reduced synthesis of a Z-scheme Ag@Fe3O4/g-C3N4 composite for photoreduction of 4-nitrophenol and photocatalytic activity. *Brazilian Journal of Chemical Engineering*. 43, 147–161. DOI: 10.1007/s43153-025-00536-5

[9] Nguyen, N.L.G., Pho, Q.-H., Nguyen, V.-C. (2016). A High Photo-Catalytic Activity of Magnetic Composite Based on Chitosan and Manganese-Doped Zinc Oxide Nanoparticles for Removal of Dyeing Wastewater. *Journal of Nanoscience and Nanotechnology,* 16(8), 7959–7967. DOI: 10.1166/jnn.2016.12763.

[10] Jawad, A.H., Abdulhameed, A.S., Surip, S.N., Alothman, Z.A. (2023). Hybrid multifunctional biocomposite of chitosan grafted benzaldehyde/montmorillonite/algae for effective removal of brilliant green and reactive blue 19 dyes: Optimization and adsorption mechanism. *Journal of Cleaner Production*, 393, 136334. DOI: 10.1016/j.jclepro.2023.136334.

[11] Guo, H., Qin, Q., Chang, J.-S., Lee, D.-J. (2023). Modified alginate materials for wastewater treatment: Application prospects. *Bioresource Technology*, 387, 129639. DOI: 10.1016/j.biortech.2023.129639.

[12] Gao, J., Li, Z., Wang, Z., Chen, T., Hu, G., Zhao, Y., Han, X. (2022). Facile Synthesis of Sustainable Tannin/Sodium Alginate Composite Hydrogel Beads for Efficient Removal of Methylene Blue. *Gels*, 8(8), 486. DOI: 10.3390/gels8080486.

[13] Duru Kamacı, U., Kamacı, M. (2024). Hydrogel beads based on sodium alginate and quince seed nanoparticles for the adsorption of methylene blue. *Inorganic Chemistry Communications*, 160, 111919. DOI: 10.1016/j.inoche.2023.111919.

[14] ALSamman, M.T., Sánchez, J. (2021). Recent advances on hydrogels based on chitosan and alginate for the adsorption of dyes and metal ions from water. *Arabian Journal of Chemistry*, 14(12), 103455. DOI: 10.1016/j.arabjc.2021.103455.

[15] Wang, Q., Gao, Q., Al-Enizi, A.M., Nafady, A., Ma, S. (2020). Recent advances in MOF-based photocatalysis: Environmental remediation under visible light. *Inorg. Chem. Front.* 7, 300–339. DOI: 10.1039/C9QI01120J.

[16] Pham, H.A. Le, Abd, A.A., Nguyen, T.H.A., Le, N.B.T., Nguyen, T.D., Nguyen, V.C., Othman, M.R. (2023). Optimization of photocatalytic degradation performance of organic dye using highly efficient bismuth MOFs: Preparation and parametric analysis. *Chem. Eng. Res. Des.*, 198, 196–207. DOI: 10.1016/j.cherd.2023.08.040.

[17] Han, Z., Yang, Y., Rushlow, J., Huo, J., Liu, Z., Hsu, Y.-C., Yin, R., Wang, M., Liang, R., Wang, K.-Y., Zhou, H.-C. (2025). Development of the design and synthesis of metal–organic frameworks (MOFs) – from large scale attempts, functional oriented modifications, to artificial intelligence (AI) predictions. *Chemical Society Reviews*, 54(1), 367–395. DOI: 10.1039/D4CS00432A.

[18] Wang, Y., Sun, H., Yang, Z., Zhu, Y., Xia, Y. (2024). Bismuth-based metal-organic frameworks and derivatives for photocatalytic applications in energy and environment: Advances and challenges. *Carbon Neutralization*, 3(4), 737–767. DOI: 10.1002/cnl2.153.

[19] Rab, S.O., Altalbawy, F.M.A., Baldaniya, L., Kumar, A., M M, R., Kundlas, M., Sharma, G.C., Joshi, K.K., Saydaxmetova, S., Abosaoda, M.K. (2025). A comprehensive review of bismuth-based photocatalysts and antibiotic pollution degradation: Recent trends and challenges. *Inorganic Chemistry Communications*, 174, 114067. DOI: 10.1016/J.INOCHE.2025.114067.

[20] Iram, S., Imran, M., Kanwal, F., Iqbal, Z., Deeba, F., Iqbal, Q.J. (2019). Bismuth(III) based Metal Organic Frameworks: Luminescence, Gas Adsorption, and Antibacterial Studies. *Zeitschrift fur Anorganische und Allgemeine Chemie*, 645(1), 50–56. DOI: 10.1002/zaac.201800383.

[21] Wang, Z., Zeng, Z., Wang, H., Zeng, G., Xu, P., Xiao, R., Huang, D., Chen, S., He, Y., Zhou, C., Cheng, M., Qin, H. (2021). Bismuth-based metal–organic frameworks and their derivatives: Opportunities and challenges. *Coordination Chemistry Reviews*, 439, 213902. DOI: 10.1016/j.ccr.2021.213902.

[22] Nguyen, V.C., Nguyen, T.D., Thanh Hoai Ta, Q., Pham, A.L.H. (2025). Hierarchical structures of GO-supported BiBTC MOFs for efficient RhB photodegradation. *RSC Adv.*, 15(4), 2779–2791. DOI: 10.1039/D4RA08337G.

[23] Pham, H.A. Le, Vo, T.K., Nguyen, D.T., Huynh, H.K., Pham, Q.T.S., Nguyen, V.C. (2022). Facile synthesis of bismuth terephthalate metal–organic frameworks and their visible-light-driven photocatalytic activities toward Rhodamine B dye. *Green Chemistry Letters and Reviews*, 15(3), 572–581. DOI: 10.1080/17518253.2022.2117998.

[24] Quang, H.T., Pham, H.A. Le, Van Cuong, N., Dang, H.P., Anh, N.T.H. (2024). Rapid Synthesis of Bismuth MOF @Carbon Nanotube Composite by microwave-assisted Solvothermal for Photodegrading RhB. *Topics in Catalysis*, 67(17–18), 1155–1168. DOI: 10.1007/s11244-024-01985-x.

[25] Eltaweil, A.S., Mamdouh, I.M., Abd El-Monaem, E.M., El-Subruiti, G.M. (2021). Highly Efficient Removal for Methylene Blue and Cu $^{2+}$ onto UiO-66 Metal–Organic Framework/Carboxylated Graphene Oxide-Incorporated Sodium Alginate Beads. *ACS Omega*, 6(36), 23528–23541. DOI: 10.1021/acsomega.1c03479.

[26] Daradmare, S., Xia, M., Le, V.N., Kim, J., Park, B.J. (2021). Metal–organic frameworks/alginate composite beads as effective adsorbents for the removal of hexavalent chromium from aqueous solution. *Chemosphere*, 270, 129487. DOI: 10.1016/j.chemosphere.2020.129487.

[27] Bui Bao Long, P., Nguyen, V.C., Pham, H.A. Le, Ta, Q.T.H., Dang, H.P. (2025). Effect of the Dimethylformamide/Isopropanol Solvent Ratio on the Structure, Optical Properties, and Photodegradation Performance of RhB Using Bi-MOF. *Bulletin of Chemical Reaction Engineering & Catalysis*, 20(1), 166–176. DOI: 10.9767/bcrec.20345.

[28] Yang, X., Zhou, T., Ren, B., Hursthouse, A., Zhang, Y. (2018). Removal of Mn (II) by Sodium Alginate/Graphene Oxide Composite Double-Network Hydrogel Beads from Aqueous Solutions. *Scientific Reports*, 8(1), 10717. DOI: 10.1038/s41598-018-29133-y.

[29] El-Desouky, M.G., Alayyafi, A.A., Al-Hazmi, G.A.A.M., El-Bindary, A.A. (2024). Effect of metal organic framework alginate aerogel composite sponge on adsorption of tartrazine from aqueous solutions: Adsorption models, thermodynamics and optimization via Box-Behnken design. *Journal of Molecular Liquids*, 399, 124392. DOI: 10.1016/j.molliq.2024.124392.

[30] Saber-Samandari, S., Saber-Samandari, S., Nezafati, N., Yahya, K. (2014). Efficient removal of lead (II) ions and methylene blue from aqueous solution using chitosan/Fe-hydroxyapatite nanocomposite beads. *Journal of Environmental Management*, 146, 481–490. DOI: 10.1016/J.JENVMAN.2014.08.010.

[31] Cheng, J., Zhan, C., Wu, J., Cui, Z., Si, J., Wang, Q., Peng, X., Turng, L.-S. (2020). Highly Efficient Removal of Methylene Blue Dye from an Aqueous Solution Using Cellulose Acetate Nanofibrous Membranes Modified by Polydopamine. *ACS Omega*, 5(10), 5389–5400. DOI: 10.1021/acsomega.9b04425.

[32] Alkaim, A.F., Aljeboree, A.M., Alrazaq, N.A., Baqir, S.J., Hussein, F.H., Lilo, A.J. (2014). Effect of pH on adsorption and photocatalytic degradation efficiency of different catalysts on removal of methylene blue. *Asian Journal of Chemistry*, 26(24), 8445–8448. DOI: 10.14233/ajchem.2014.17908.

[33] Vu, T.T.H., Bui, T.D., Nguyen, L.H.K., Nguyen, T.H.A. (2025). Polyethyleneimine-Functionalized Magnetic Bagasse Composite for Efficient Adsorptive Removal of Yellow 4GL and Black R–S Dyes. *Bulletin of Chemical Reaction Engineering & Catalysis*, 20(2), 318–330. DOI: 10.9767/bcrec.20368.

[34] Eldin, M.S.M., Soliman, E.A., Elzatahry, A.A.F., Elaassar, M.R., Eweida, B.Y., Elkady, M.F., Rahman, A.M.A., Yossef, M.E. (2019). Carboxylated alginate hydrogel beads for methylene blue removal: formulation, kinetic and isothermal studies. *Desalination and Water Treatment*, 168, 308–323. DOI: 10.5004/dwt.2019.24628.

[35] Chen, T., Liu, H., Gao, J., Hu, G., Zhao, Y., Tang, X., Han, X. (2022). Efficient Removal of Methylene Blue by Bio-Based Sodium Alginate/Lignin Composite Hydrogel Beads. *Polymers*, 14(14), 2917. DOI: 10.3390/polym14142917.

[36] Farasati Far, B., Naimi-Jamal, M.R., Jahanbakhshi, M., Keihankhadiv, S., Baradarbarjastehbaf, F. (2024). Enhanced methylene blue adsorption using single-walled carbon nanotubes/chitosan-graft-gelatin nanocomposite hydrogels. *Scientific Reports*, 14(1), 19217. DOI: 10.1038/s41598-024-69969-1.

[37] Zhang, Z.-H., Xu, J.-Y., Yang, X.-L. (2021). MXene/sodium alginate gel beads for adsorption of methylene blue. *Materials Chemistry and Physics*, 260, 124123. DOI: 10.1016/j.matchemphys.2020.124123.